
COMPARATIVE CLINICAL EVALUATION OF “MEMORY-EFFICIENT” SYNTHETIC 3D GENERATIVE ADVERSARIAL NETWORKS (GAN) HEAD-TO-HEAD TO STATE OF ART: RESULTS ON COMPUTED TOMOGRAPHY OF THE CHEST

Mahshid Shiri¹, Chandra Bortolotto², Alessandro Bruno³, Alessio Consonni⁴, Daniela Maria Grasso⁴,
Leonardo Brizzi⁴, Daniele Loiacono¹, Lorenzo Preda²

¹ Dipartimento di Elettronica, Informazione e Bioingegneria, Politecnico di Milano, Milan, Italy

² Radiology Institute, Fondazione IRCCS Policlinico San Matteo Pavia - Università degli studi di Pavia, Italy

³ Department of Business Law Economics, Consumer Behavior “Carlo A. Ricciardi”, Faculty of Communication, IULM University, Milan, Italy

⁴ Radiology Institute, Fondazione IRCCS Policlinico San Matteo Pavia, Italy

ABSTRACT

Introduction: Generative Adversarial Networks (GANs) are increasingly used to generate synthetic medical images, addressing the critical shortage of annotated data for training Artificial Intelligence (AI) systems. This study introduces a novel memory-efficient GAN architecture, incorporating Conditional Random Fields (CRFs) to generate high-resolution 3D medical images and evaluates its performance against the state-of-the-art hierarchical (HA)-GAN model.

Materials and Methods: The CRF-GAN was trained using the open-source lung CT LUNA16 dataset. The architecture was compared to HA-GAN through a quantitative evaluation, using Fréchet Inception Distance (FID) and Maximum Mean Discrepancy (MMD) metrics, and a qualitative evaluation, through a two-alternative forced choice (2AFC) test completed by a pool of 12 resident radiologists, in order to assess the realism of the generated images.

Results: CRF-GAN outperformed HA-GAN with lower FID (0.047 vs. 0.061) and MMD (0.084 vs. 0.086) scores, indicating better image fidelity. The 2AFC test showed a significant preference for images generated by CRF-GAN over those generated by HA-GAN with a p-value of 1.93e-05. Additionally, CRF-GAN demonstrated 9.34% lower memory usage at 256³ resolution and achieved up to 14.6% faster training speeds, offering substantial computational savings.

Discussion: CRF-GAN model successfully generates high-resolution 3D medical images with non-inferior quality to conventional models, while being more memory-efficient and faster. Computational power and time saved can be used to improve the spatial resolution and anatomical accuracy of generated images, which is still a critical factor limiting their direct clinical applicability.

Keywords: Generative Adversarial Networks – Artificial Intelligence – CT synthesis – Deep Learning

1 Introduction

Artificial Intelligence (AI) systems are proving to be valuable tools for supporting radiologists in the diagnostic process. They may be especially helpful in the interpretation of medical images, improving diagnostic accuracy and the timeliness of therapeutic interventions [2]. However, the success of these systems and their widespread implementation in clinical settings is still limited by the availability of large datasets with annotated medical data, which are essential for their training [3]. Annotated medical data from experts is often difficult to obtain due to privacy concerns, high costs, complexity of collection procedures, and the need for approval by ethical committees [4]. In light of these challenges, the expansion of datasets with synthetic labeled data is of increasing interest to researchers and clinicians.

Previous models for dataset expansion were represented by Data Augmentation systems, such as intensity transformations, rotation, translation, cropping, and other geometric transformations [4,5]. However, these methods had limitations in capturing the heterogeneity of real image distributions, as they generated images through a one-to-one process. In this context of scarcity of quality data, Generative Adversarial Networks (GANs) [6] offer a promising solution. By learning the characteristics and distributions of real data, GANs can generate realistic and entirely new medical images that replicate the variability and complexity of images used in clinical practice. This enables the training of more robust and accurate AI systems. GANs, whose classic architecture was proposed in 2014, consist of two deep neural networks: the Generator and the Discriminator. These two networks operate simultaneously in a minimax game. The Generator creates new data samples, while the Discriminator evaluates both generated and real samples, aiming to distinguish between them. This ongoing competition drives both components to improve their performances. 3D GAN models have been proposed for various applications, including reducing noise in low-dose CT scans [7], enhancing the quality of CT images [8], generating realistic 3D brain MRI images [9], and creating tumor masks for segmentation [10]. In the specific area of CT image generation, Ferreira et al. [11] and Han et al. [5] aimed to synthesize realistic 3D images of lung parenchyma or lung nodules using different 3D GAN models: Progressive Growing (PG)-GAN in [11] and a Multi-Conditional (MC)-GAN in [5]. However, these methods have a limitation in the generated image resolution, which is usually 128^3 or smaller, because of limited memory during training [12].

Memory-efficient GANs seek to balance memory efficiency and generative capability, ensuring effective GAN training even with limited computational resources. To achieve this, Lei et al. [13] and Yu et al. [14] focused on generating new images slice-by-slice or patch-by-patch. However, as these methods generate patches and slices independently, potentially leading to artifacts at the boundaries. Also, Uzunova et al. [15] uses two GANs for image generation, with the first network producing a lower-resolution version and the second generating higher-resolution patches conditioned on the first GAN's output. This approach remains patch-based and lacks a comprehensive understanding of the entire image structure. Furthermore, Sun et al. [12] introduced an end-to-end hierarchical GAN architecture (HA-GAN) capable of generating high-resolution 3D images at a resolution of 256^3 . HA-GAN comprises two interconnected GANs: a low-resolution GAN that produces a low-resolution version of the 3D image, capturing the essential global structure with reduced computational and memory demands, and a high-resolution GAN that generates high-resolution patches for a randomly selected sub-volume of the image. HA-GAN [12] has shown superior performance compared to several baseline models, including WGAN [21], VAE-GAN [22], α GAN [23], ProgressiveGAN [24], 3D StyleGAN 2 [25], and CCE-GAN [26]. Additionally, HA-GAN is the only model that can generate images at a resolution of 256^3 , overcoming memory constraints that limit other models. For this reason, our proposed architecture is compared directly to HA-GAN.

This work addresses the limitations of existing 3D GAN models by proposing a novel “memory-efficient” architecture for high-resolution 3D medical image synthesis. This architecture combines Conditional Random Fields (CRFs) with GANs to reduce memory usage while improving performance. CRF is a probabilistic graphical model that models dependencies between output variables, considering the sequential or structural nature of the data. CRFs enable the capture of correlations between image patches. The unary potential in a CRF represents the likelihood of assigning a particular label to a patch based solely on its features, while the pairwise potential considers the relationship between neighboring patches, encouraging label consistency in adjacent regions and capturing the spatial structure and dependencies within the image.

The primary contribution of this work is to assess the clinical realism of synthetic images generated by memory-efficient GANs. This process is crucial for validating the practicality and applicability of these images in real-world medical settings, thereby enhancing the potential of AI-driven healthcare solutions. The contributions of this work may be summarized as follows:

1. We present a novel, memory-efficient architecture by incorporating CRFs into the middle layers of GANs to capture anatomical structures, aiming to increase consistency in the synthetic images.
2. We assessed and analyzed the clinical value of the synthetic CRF-GAN images by comparing them, through qualitative and quantitative evaluation, with synthetic images from another GAN model (HA-GAN) used as a “competitor.” The goal of this evaluation is to assess the non-inferiority of CRF-GAN:
 - (a) From a qualitative perspective (primary endpoint)
 - (b) From a quantitative perspective (secondary endpoint)

2 Materials and Methods

2.1 Datasets

The study utilizes a publicly accessible 3D dataset employed for the Lung Nodule Analysis 2016 (LUNA16) challenge [18] which is a subset of the LIDC-IDRI dataset [19]. The Lung Image Database Consortium image collection (LIDC-IDRI) constitutes diagnostic thoracic computed tomography (CT) scans annotated with marked lesions. It serves as an internationally accessible resource for the development, training, and evaluation of AI systems for lung cancer detection and diagnosis. Initiated by the National Cancer Institute and further advanced by the Foundation for the National Institutes of Health, this is public-private partnership, accompanied by the Food and Drug Administration. This dataset comprises 1018 cases [19].

A subset of the LIDC-IDRI database, publicly accessible, was utilized for the LUNA16 challenge [18]. CT scans with a slice thickness exceeding 2.5 mm were excluded, resulting in a total of 888 CT scans for analysis. The entire dataset was partitioned into 10 subsets, accessible as compressed zip files. Within each subset, CT images are stored in MetaImage (mhd/raw) format.

The dataset was divided into two subsets, allocating 90% for training and 10% for validation.

During the preprocessing phase, in line with the approach of [12], blank axial slices are eliminated by substituting them with zero values. Subsequently, the images are resized to dimensions of 256^3 . Additionally, the Hounsfield units (HU) of the images undergo calibration, and air density correction is applied. To ensure uniformity, the HU are mapped to the intensity window of $[-1024, 600]$, and normalized to the range $[-1, 1]$.

2.2 Model

Model Description:

The proposed architecture introduces a novel two-step GAN framework, using CRFs for improved image synthesis by emphasizing consistency and structural coherence. GANs typically refine an image progressively across their layers, with initial layers generating coarse structures and later layers fine-tuning details. The generator in this architecture is divided into two components: the first part generates an embedding that encapsulates the image's global structure, while the second refines this embedding into high-resolution image patches. To achieve memory efficiency, the second part processes only a subset of the embedding during training, generating patches of the image rather than the entire output. This selective approach reduces computational overhead. During inference, the second part of the generator utilizes the complete embedding to produce a full-resolution image, ensuring that the final output is both structurally consistent and visually detailed. A critical innovation here is the application of CRFs to these embeddings, enabling the model to enhance inter-patch consistency without the computational overhead of training an additional GAN [12].

The architecture also incorporates a "half-encoder" to further reinforce the generator's consistency and prevent mode collapse. This encoder takes image as input and generates embeddings that are compared to the original ones during training. By focusing on embedding correlations, the CRF enhances the generator's ability to produce structurally coherent and realistic images. During training, a dual-feedback mechanism operates: the CRF ensures structural alignment within the embeddings, while the discriminator evaluates the realism of the output image patches. This lightweight and memory-efficient approach improves the generator's ability to synthesize consistent and high-quality images.

The two-step GAN structure and CRF integration present a significant advance in generative modeling, offering a lower computational footprint compared to traditional methods. The overall architecture is illustrated in Figure 1.

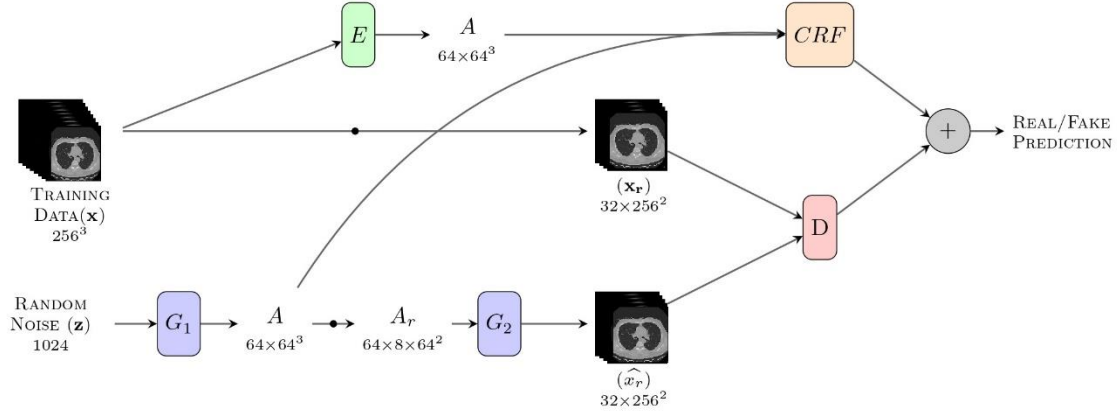


Figure 1 CRF-GAN Architecture.

The proposed CRF-GAN architecture was implemented using PyTorch, incorporating 3D CNN layers for image synthesis. The model was trained for 80 epochs on a TITAN V GPU with 12 GB of memory. The Adam optimizer was employed for training due to its adaptive learning rate properties. The training process utilized binary cross-entropy loss for binary classification tasks. Additionally, L1Loss was employed for the encoder, promoting sharper and more detailed outputs. The discriminator's architecture integrated spectral normalization to stabilize GAN training, while the generator leveraged transposed convolutional layers with batch normalization and ReLU activation. The encoder employed 3D convolutional layers and group normalization. The hyperparameters were the same as [12].

2.3 Evaluation

The comparison with HA-GAN has been conducted from both a quantitative and qualitative perspective, while the performance evaluation also considers key parameters such as maximum memory usage, the number of learnable parameters, and training speed. The evaluation procedures employed are detailed below.

2.3.1 Quantitative Evaluation

To evaluate the synthetic images generated by two models, we used two key metrics: Fréchet Inception Distance (FID) and Maximum Mean Discrepancy (MMD).

Heusel et al. [27] introduced the Fréchet Inception Distance (FID) as a metric for assessing the quality of generated samples. FID accomplishes this by embedding a set of generated samples into a feature space provided by a specific layer of Inception Net or any Convolutional Neural Network (CNN). The embedding layer is treated as a continuous multivariate Gaussian, and both the mean and covariance are estimated for the generated and real data. The Fréchet distance, also known as the Wasserstein-2 distance, between these two Gaussian distributions is then utilized to quantify the quality of the generated samples. A lower FID value indicates smaller distances between the synthetic and real data distributions. FID is recognized for its ability to discriminate between samples, its robustness, and its computational efficiency. Although FID is considered a reliable measure, it assumes that the features follow a Gaussian distribution, which may not always hold true. The FID metric degrades as various types of artifacts are introduced into the images. This score aligns well with human judgments and focuses on measuring the dissimilarity between the generated and real distributions.

The measure known as MMD calculates the difference between two probability distributions by using independently drawn samples from each distribution [28]. A lower MMD value indicates that two distributions are closer. MMD can be considered as a two-sample testing method (i.e. Distinguishing two distributions by finite samples), which tests whether one model or another is closer to the true data distribution.

Overall, FID measures how closely the generated images match the real image distribution, accounting for both precision and recall. MMD, on the other hand, assesses the difference between real and generated images with minimal sample and computational complexity. Lower FID and MMD values indicate that the generated images closely resemble real images.

2.3.2 Qualitative Evaluation

The qualitative evaluation of images aims to assess the clinical value of the synthetic CRF-GAN images by evaluating their realism from a purely subjective standpoint rather than using objective metrics. The evaluation was performed by a pool of twelve (12) resident radiologists, working at IRCCS San Matteo of Pavia, with experience dealing with chest CT imaging. The majority of them (9/12, 75%), at the time of evaluation, were attending the fourth and last year of residency, one of them (8,34%) was attending the third year of residency and two of them (16,67%) were attending the second year of residency. All the residents involved already completed the chest CT internal rotation of six months, assuming that they were equally experienced on that specific topic and could provide evaluation on thoracic imaging with the same amount of expertise. The evaluation was conducted through a two alternative forced choice (2AFC) test composed of two sections:

1. In the first section, the evaluator was presented with a total of 10 questions each presenting two sets of randomly selected images from a chest CT scan, acquired at the same slice (position) on the same anatomical plane (axial, coronal or sagittal). One of the two images had been artificially generated using CRF-GAN model, while the other was a real CT, resized at a 256^3 resolution to match the resolution of the generated image, but no information about their origin was provided.

The task of the evaluator was to identify which image was the real one. Subsequently, the evaluator had to assess the level of difficulty of the task using a Likert scale from 1 (extremely subtle) to 5 (obvious).

2. In the second section, the evaluator was presented with 30 questions displaying two randomly selected slices of chest CT images each, acquired at the same position and on the same anatomical plane; both images of each pair had been artificially generated, one from CRF-GAN model and the other one from HA-GAN model. The evaluator's task was to indicate the most realistic one.

The test had to be completed in one sitting as it was not possible to pause and resume later to avoid any bias.

To determine the statistical significance of the preference for CRF-GAN or HA-GAN through our study, we used chi-square test.

2.3.3 Computational Performance Evaluation

For computational performance evaluation, we used a test set consisting of 10% of the LUNA16 dataset, with all experiments conducted at a resolution of 256^3 . To evaluate the model's complexity and efficiency, we monitored the maximum memory usage during training with batch sizes of 2, 4, and 6. Furthermore, to enhance our evaluation, we quantified the total number of learnable parameters within the models to assess their complexity, as a higher number of parameters necessitates a larger dataset. This consideration is particularly significant in clinical applications since medical datasets are often limited in size compared to those of natural images. Additionally, we measured the training speed of the models by conducting training over 1000 iterations and determining the average number of iterations completed per second.

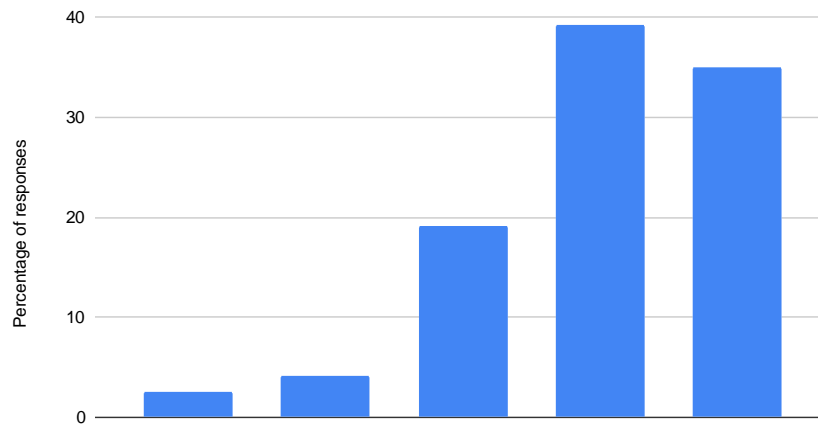


Figure 2 The graph displays the difficulty scores for identifying real and synthetic images. The y-axis shows the percentage of responses for each score, while the x-axis represents the range of difficulty scores with 1: 'Extremely Subtle', 2: 'Moderately Subtle', 3: 'Fairly Subtle', 4: 'Moderately Obvious' and 5: 'Obvious'.

Table 1: FID and MMD scores computed on the 256³ resolution images of GSP and LUNA16 dataset. As lower FID and MMD scores outline better image fidelity, it can be seen that CRF-GAN achieved better results.

Models	LUNA16 dataset	
	FID ↓	MMD ↓
HA-GAN	0.061021	0.086461
CRF-GAN	0.047062	0.084015

3 Results

3.1 Quantitative results: FID and MMD scores

Lower FID and MMD scores serve as indicators of the proximity of generated images to real images, reflecting the performance of the models. These scores are calculated on 256³ resolution of the synthetic images produced by CRF-GAN and HA-GAN and are presented in Table 1, with CRF-GAN outperforming HA-GAN in terms of both metrics.

3.2 Qualitative results: 2AFC test

In the first section of the test, we compared real and synthetic images. All twelve experts correctly identified all real images for every question which shows that the synthetic images are not identical with real ones. Analyzing the difficulty ratings reveals that synthetic images rarely posed challenges for the experts as can be seen in Figure 2.

This study also aimed to compare the performance of two synthetic image generation models, CRF-GAN and HA-GAN. Figure 3 presents examples of image pairs, illustrating that in some instances HA-GAN was preferred more frequently, while in others, CRF-GAN received a higher number of selections. The study focused on quantifying participant preferences and analyzing the statistical significance of these preferences between the two models. Descriptive statistics in Table 2 provide an overview of the total votes received by each model, as well as the average and variability in votes per image pair.

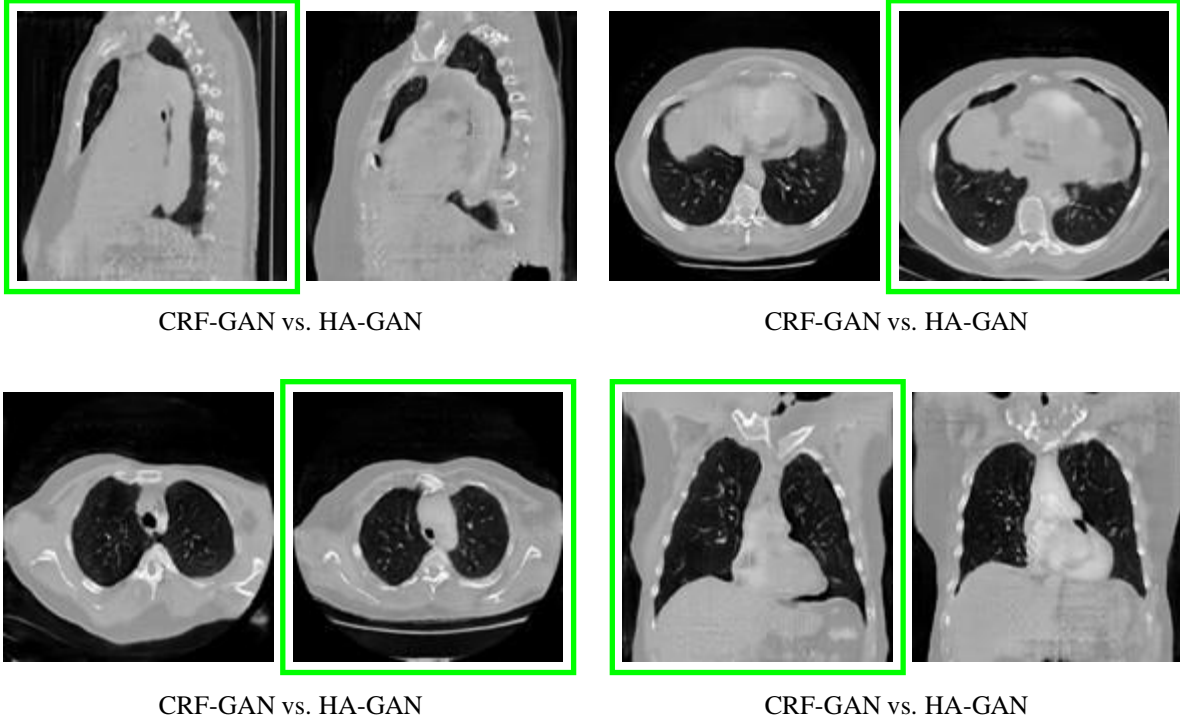


Figure 3 Sample pairs from the 2AFC test. The image pair that was chosen more often as realistic is bounded with a green box (CRF-GAN on the left, HA-GAN on the right).

Table 2: Descriptive Statistics of Votes

Statistic	Value
Total Votes for CRF-GAN	215
Total Votes for HA-GAN	145
Mean Votes for CRF-GAN per Pair	7.16
Mean Votes for HA-GAN per Pair	4.83
Standard Deviation of Votes for CRF-GAN	2.66
Standard Deviation of Votes for HA-GAN	2.66
Chi-square (p-value)	71.42 (1.93e-05)

3.3 Computational Performance Evaluation

3.3.1 Model Complexity:

We explored the complexity of CRF-GAN and HA-GAN models by analyzing the total number of learnable parameters at different resolutions, which are presented in Table 3. The proposed model demonstrates a reduction in parameters at each resolution, with decreases of 27.4%, 28.1%, and 28.2% observed for resolutions 64^3 , 128^3 , and 256^3 respectively, as highlighted in the table.

Table 3: The parameter counts for CRF-GAN and HA-GAN at varying resolutions, which are indicated in millions (M) in the table.

Resolution	#Parameters	
	CRF-GAN	HA-GAN
64^3	57.07 M	78.7 M
128^3	57.20 M	79.58 M
256^3	57.24 M	79.74 M

In addition, we measured the number of iterations per second during training, setting the batch size to 2. The comparison was conducted at 128^3 and 256^3 resolutions. The results indicate that at a 256^3 resolution, CRF-GAN achieves a training speed of 1.394 iterations per second, whereas HA-GAN achieves 1.216 iterations per second. This means CRF-GAN is approximately 14.6% faster than HA-GAN at this resolution. At a 128^3 resolution, CRF-GAN achieves 4.236 iterations per second, while HA-GAN achieves 3.845 iterations per second, making CRF-GAN about 10.2% faster at this lower resolution.

3.3.2 Memory efficiency:

In order to compare memory usage, we captured the maximum memory allocated by each model during training. This procedure was performed on batch sizes of 2, 4, and 6 on both 128^3 and 256^3 resolutions. The results are outlined in Table 4.

As it can be seen, HA-GAN consistently demanded more memory resources than CRF-GAN across different resolutions and batch sizes. On average, HA-GAN utilized approximately 9.65% more memory compared to CRF-GAN at 128^3 resolution and approximately 9.34% more memory at 256^3 resolution.

Table 4: Memory usage (in MB) of HA-GAN and CRF-GAN for different batch sizes at 128^3 and 256^3 resolutions. "-" indicates that the models exceed GPU memory.

Models	128^3			256^3		
	2	4	6	2	4	6
HA-GAN	2812	2984	3098	7710	10434	—
CRF-GAN	2622	2712	2774	7494	9010	—

4 Discussion

Memory-efficient 3D GANs may facilitate data generation while utilizing minimal computational resources, thereby expanding datasets to mitigate data scarcity; these models, increasing iterations and so image quality without increasing generation time, may not only save time and resources but also uphold a high standard of data quality.

While in literature most works focused on presenting 3D GAN models generating only specific anatomical parts [11, 5], or patch-based architecture prone to artifacts [13, 14, 15], in our knowledge only Sun et al. [12] introduced a low computational and memory demanding high-resolution 3D GAN architecture outperforming state-of-art models that generate coherent high-resolution 3D images, called HA-GAN.

In this work, we proposed a novel memory-efficient architecture for high-resolution 3D medical image synthesis thanks to the implementation of Conditional Random Fields and we assessed the clinical value of the synthetic images by comparing them, through qualitative (endpoint 1) and quantitative (endpoint 2) evaluation.

From a computational performance and workload point of view, CRF-GAN proved to be a lighter model than HA-GAN, both in terms of learnable parameters and memory usage. The significantly fewer learnable parameters of CRF-GAN compared to HA-GAN, leads to higher computational efficiency during training, reflecting in a larger number of iterations per second at both 128^3 and 256^3 resolution. Regarding memory usage, HA-GAN consistently demanded more memory resources than CRF-GAN across different resolutions and batch sizes. Interestingly, as the batch size increased, this percentage difference tended to increase at both resolutions, indicating that higher batch sizes amplify the disparity in memory usage between the two models.

In terms of quantitative evaluation, both FID and MMD metrics values show better image fidelity for CRF-GAN. Quantitative metrics are essential for objectively assessing the quality of images generated by synthesis models, as they measure the discrepancy between the distributions of real and synthetic images. However, relying solely on these metrics can be misleading due to their inherent limitations. For instance, FID assumes a Gaussian distribution of the features extracted from the images, which is not always true, thereby compromising the reliability of the evaluation. Similarly, MMD quantifies the difference between two probability distributions but does not provide information on which specific features contribute to this difference, limiting the interpretability of the results. Therefore, it is crucial to complement these metrics with qualitative assessments to adopt a holistic approach that allows for a deeper understanding of the quality of the generated images.

In terms of qualitative assessment process, the 2AFC test allowed radiologists residents to formulate some subjective, but globally shared, evaluations on the clinical nature of the images, stemming from their expertise in the field of medical radiology. The qualitative difference, evident in comparison with real images, is not evident in comparison with the generated ones: The correctness of this assumption is confirmed by the results of the 2AFC test. The result of the 2AFC test shows a clear preference for CRF-GAN over HA-GAN. Out of the total votes, CRF-GAN received 215 (59,7%), while HA-GAN garnered 145, indicating that participants were more likely to choose images from CRF-GAN as appearing more realistic. On average, CRF-GAN received 7.16 votes per image pair, compared to HA-GAN's 4.83. Both models showed similar variability in votes with a standard deviation of 2.66. A chi-square test was performed to assess the statistical significance of this preference. The test yielded a chi-square statistic of 71.42 with an extremely low p-value of $1.93e-05$, demonstrating that the observed difference is highly unlikely to be due to random chance. This indicates a strong and statistically significant preference for CRF-GAN over HA-GAN in terms of generating more realistic images.

However, there remains a significant gap between the current capabilities of GAN-generated images (HA- or CRF-) and their practical application in real-world clinical settings as the qualitative distance between generated and real images is still evident, both in terms of spatial resolution and anatomical accuracy. While the qualitative difference is undeniable, it is yet to be determined whether a poor performance from a purely clinical or subjective perspective correlates with limitations in quantitative metrics. This question can guide future studies aimed at evaluating the performance of AI systems trained on medical datasets, while also exploring the potential of using 3D GAN models for data augmentation to improve diagnostic accuracy.

There are some limitations to this study. The number of participants (twelve) may restrict the generalization of the results. Additionally, participant bias could be introduced, as individual criteria for evaluating image quality vary among the participants, potentially affecting the outcomes. The resolution at which the images were generated (256^3) represents a step forward from the point of view of 3D generative models, as already discussed in previous sections. However, in the clinical-radiological field, this resolution does not reflect the one usually used, which is normally 512^3 or higher, depending on the CT scanner setting used. Furthermore, it should be noted that this aspect did not represent a bias in the comparison of the generated images with real ones since the real images were downsampled to a 256^3 resolution, making them comparable with the generated ones. Also, we evaluated only the GAN's capability of generating chest CT volumes

with no pathological findings. Since AI systems need to be trained on lung’s nodules, further studies are needed in which the GAN’s ability to generate pathological findings is explored. Moreover, although both CRF-GAN and HA-GAN are 3D models, the quality evaluation by residents has been conducted on 2D slices randomly selected from the generated volume. This procedure doesn’t follow the usual CT scan interpretation method in an everyday clinical context, made of scrollable volumes. However, it’s uncertain if a different test design with 3D scrollable volumes could provide different results. Furthermore, we evaluated the clinical value of memory-efficient CRF-GANs, but additional paradigms, such as variational auto-encoders (VAEs) [31] and normalizing flows [32], should be considered in future work.

5 Conclusion

Memory-efficient GANs such as CRF-GAN both on qualitatively and qualitatively evaluation results to be non-inferior to conventional state-of-the-art ones. Their generative effectiveness can provide significant benefits in correcting data scarcity and fragmentation present in datasets dedicated to training AI systems as well as making it possible to allocate saved computational power to reduce production time, increase quality, or make easier local generation and federated learning.

The authors declare that no funds, grants, or other support were received during the preparation of this manuscript.

The authors have no relevant financial or non-financial interests to disclose.

References

- [1] D Douglas Miller and Eric W Brown. Artificial intelligence in medical practice: the question to the answer? *The American journal of medicine*, 131(2):129–133, 2018.
- [2] Zechen Zheng, Miao Wang, Chao Fan, Congqian Wang, Xuelei He, and Xiaowei He. Light&fast generative adversarial network for high-fidelity ct image synthesis of liver tumor. *Computer Methods and Programs in Biomedicine*, page 108252, 2024.
- [3] Youssef Skandarani, Pierre-Marc Jodoin, and Alain Lalande. Gans for medical image synthesis: An empirical study. *Journal of Imaging*, 9(3):69, 2023.
- [4] José Mendes, Tania Pereira, Francisco Silva, Julieta Frade, Joana Morgado, Cláudia Freitas, Eduardo Negrão, Beatriz Flor De Lima, Miguel Correia Da Silva, António J Madureira, et al. Lung ct image synthesis using gans. *Expert Systems with Applications*, 215:119350, 2023.
- [5] Changhee Han, Yoshiro Kitamura, Akira Kudo, Akimichi Ichinose, Leonardo Rundo, Yujiro Furukawa, Kazuki Umemoto, Yuanzhong Li, and Hideki Nakayama. Synthesizing diverse lung nodules wherever massively: 3d multi-conditional gan-based ct image augmentation for object detection. In *2019 International Conference on 3D Vision (3DV)*, pages 729–737. IEEE, 2019.
- [6] Ian Goodfellow, Jean Pouget-Abadie, Mehdi Mirza, Bing Xu, David Warde-Farley, Sherjil Ozair, Aaron Courville, and Yoshua Bengio. Generative adversarial nets. *Advances in neural information processing systems*, 27, 2014.
- [7] Hongming Shan, Yi Zhang, Qingsong Yang, Uwe Kruger, Mannudeep K Kalra, Ling Sun, Wenxiang Cong, and Ge Wang. 3-d convolutional encoder-decoder network for low-dose ct via transfer learning from a 2-d trained network. *IEEE transactions on medical imaging*, 37(6):1522–1534, 2018.
- [8] Akira Kudo, Yoshiro Kitamura, Yuanzhong Li, Satoshi Iizuka, and Edgar Simo-Serra. Virtual thin slice: 3d conditional gan-based super-resolution for ct slice interval. In *Machine Learning for Medical Image Reconstruction: Second International Workshop, MLMIR 2019, Held in Conjunction with MICCAI 2019, Shenzhen, China, October 17, 2019, Proceedings 2*, pages 91–100. Springer, 2019.
- [9] Weina Jin, Mostafa Fatehi, Kumar Abhishek, Mayur Mallya, Brian Toyota, and Ghassan Hamarneh. Applying artificial intelligence to glioma imaging: Advances and challenges. *arXiv preprint arXiv:1911.12886*, pages 1–31, 2019.
- [10] Marco Domenico Cirillo, David Abramian, and Anders Eklund. Vox2vox: 3d-gan for brain tumour segmentation. In *Brainlesion: Glioma, Multiple Sclerosis, Stroke and Traumatic Brain Injuries: 6th International Workshop, BrainLes 2020, Held in Conjunction with MICCAI 2020, Lima, Peru, October 4, 2020, Revised Selected Papers, Part I 6*, pages 274–284. Springer, 2021.
- [11] Artur Ferreira, Tania Pereira, Francisco Silva, Ana T Vilares, Miguel C Silva, António Cunha, and Hélder P Oliveira. Synthesizing 3d lung ct scans with generative adversarial networks. In *2022 44th Annual International Conference of the IEEE Engineering in Medicine & Biology Society (EMBC)*, pages 2033–2036. IEEE, 2022.
- [12] Li Sun, Junxiang Chen, Yanwu Xu, Mingming Gong, Ke Yu, and Kayhan Batmanghelich. Hierarchical amortized gan for 3d high resolution medical image synthesis. *IEEE journal of biomedical and health informatics*, 26(8):3966–3975, 2022.
- [13] Yang Lei, Tonghe Wang, Yingzi Liu, Kristin Higgins, Sibao Tian, Tian Liu, Hui Mao, Hyunsuk Shim, Walter J Curran, Hui-Kuo Shu, et al. Mri-based synthetic ct generation using deep convolutional neural network. In *Medical Imaging 2019: Image Processing*, volume 10949, pages 716–721. SPIE, 2019.
- [14] Biting Yu, Luping Zhou, Lei Wang, Jurgen Frapp, and Pierrick Bourgeat. 3d cgan based cross-modality mr image synthesis for brain tumor segmentation. In *2018 IEEE 15th international symposium on biomedical imaging (ISBI 2018)*, pages 626–630. IEEE, 2018.
- [15] Hristina Uzunova, Jan Ehrhardt, Fabian Jacob, Alex Frydrychowicz, and Heinz Handels. Multi-scale gans for memory-efficient generation of high resolution medical images. In *Medical Image Computing and Computer Assisted Intervention–MICCAI 2019: 22nd International Conference, Shenzhen, China, October 13–17, 2019, Proceedings, Part VI 22*, pages 112–120. Springer, 2019.
- [16] Jing Gao, Wenhan Zhao, Peng Li, Wei Huang, and Zhikui Chen. Legan: A light and effective generative adversarial network for medical image synthesis. *Computers in Biology and Medicine*, 148:105878, 2022.
- [17] Randy L. Buckner, Joshua L. Roffman, and Jordan W. Smoller. Brain Genomics Superstruct Project (GSP), 2014.
- [18] Arnaud Arindra Adiyoso Setio, Alberto Traverso, Thomas De Bel, Moira SN Berens, Cas Van Den Bogaard, Piergiorgio Cerello, Hao Chen, Qi Dou, Maria Evelina Fantacci, Bram Geurts, et al. Validation, comparison, and

- combination of algorithms for automatic detection of pulmonary nodules in computed tomography images: the luna16 challenge. *Medical image analysis*, 42:1–13, 2017.
- [19] Samuel G Armato III, Geoffrey McLennan, Luc Bidaut, Michael F McNitt-Gray, Charles R Meyer, Anthony P Reeves, Binsheng Zhao, Denise R Aberle, Claudia I Henschke, Eric A Hoffman, et al. The lung image database consortium (lidc) and image database resource initiative (idri): a completed reference database of lung nodules on ct scans. *Medical physics*, 38(2):915–931, 2011.
 - [20] Yi Li and Wei Ping. Cancer metastasis detection with neural conditional random field. *arXiv preprint arXiv:1806.07064*, 2018.
 - [21] Ishaan Gulrajani, Faruk Ahmed, Martin Arjovsky, Vincent Dumoulin, and Aaron C Courville. Improved training of wasserstein gans. *Advances in neural information processing systems*, 30, 2017.
 - [22] Anders Boesen Lindbo Larsen, Søren Kaae Sønderby, Hugo Larochelle, and Ole Winther. Autoencoding beyond pixels using a learned similarity metric. In *International conference on machine learning*, pages 1558–1566. PMLR, 2016.
 - [23] Gihyun Kwon, Chihye Han, and Dae-shik Kim. Generation of 3d brain mri using auto-encoding generative adversarial networks. In *International Conference on Medical Image Computing and Computer-Assisted Intervention*, pages 118–126. Springer, 2019.
 - [24] Tero Karras, Timo Aila, Samuli Laine, and Jaakko Lehtinen. Progressive growing of gans for improved quality, stability, and variation. arxiv 2017. *arXiv preprint arXiv:1710.10196*, pages 1–26, 2018.
 - [25] Sungmin Hong, Razvan Marinescu, Adrian V Dalca, Anna K Bonkhoff, Martin Bretzner, Natalia S Rost, and Polina Golland. 3d-stylegan: A style-based generative adversarial network for generative modeling of three-dimensional medical images. In *Deep Generative Models, and Data Augmentation, Labelling, and Imperfections: First Workshop, DGM4MICCAI 2021, and First Workshop, DALI 2021, Held in Conjunction with MICCAI 2021, Strasbourg, France, October 1, 2021, Proceedings 1*, pages 24–34. Springer, 2021.
 - [26] Shibo Xing, Harsh Sinha, and Seong Jae Hwang. Cycle consistent embedding of 3d brains with auto-encoding generative adversarial networks. In *Medical Imaging with Deep Learning*, 2021.
 - [27] Martin Heusel, Hubert Ramsauer, Thomas Unterthiner, Bernhard Nessler, and Sepp Hochreiter. Gans trained by a two time-scale update rule converge to a local nash equilibrium. *Advances in neural information processing systems*, 30, 2017.
 - [28] Robert Fortet and Edith Mourier. Convergence de la répartition empirique vers la répartition théorique. In *Annales scientifiques de l’École Normale Supérieure*, volume 70, pages 267–285, 1953.
 - [29] Gretton A Borgwardt KM Rasch MJ. Schölkopf b smola a a kernel two-sample test. *J. Mach. Learn. Res*, 13(1):723, 2012.
 - [30] Gao Huang, Yang Yuan, Qiantong Xu, Chuan Guo, Yu Sun, Felix Wu, and Kilian Weinberger. An empirical study on evaluation metrics of generative adversarial networks. 2018.
 - [31] Danilo Jimenez Rezende, Shakir Mohamed, and Daan Wierstra. Stochastic backpropagation and approximate inference in deep generative models. In *International conference on machine learning*, pages 1278–1286. PMLR, 2014.
 - [32] Laurent Dinh, Jascha Sohl-Dickstein, and Samy Bengio. Density estimation using real nvp. *arXiv preprint arXiv:1605.08803*, 2016.